SPECIAL PROJECT FINAL REPORT

All the following mandatory information needs to be provided.

Project Title:	FLEXPART transport simulations and inverse modelling of atmospheric components
Computer Project Account:	spnoflex
Start Year - End Year :	2017 – 2019
Principal Investigator(s)	Espen Sollum
Affiliation/Address:	NILU- Norwegian Institute for Air Research NILU – Norwegian Institute for Air Research PO box 100 NO-2027 Kjeller
Other Researchers (Name/Affiliation):	Sabine Eckhardt, Massimo Cassiani, Rona Thompson, Thomas Hamburger, Henrik Grythe, Ignacio Pisso, Arve Kylling, Andreas Stohl

The following should cover the entire project duration.

Summary of project objectives

(10 lines max)

The Lagrangian particle dispersion model FLEXPART is run on ECMWF data to explore the transport and dispersion of various atmospheric constituents from greenhouse gases, aerosols like black carbon to volcanic ash released during eruptions. The model is used with various inversion techniques to infer emission estimates of many atmospheric compounds. This helps improving transport simulations of these substances and to understand their contribution and effects on the climate system.

Summary of problems encountered

(If you encountered any problems of a more technical nature, please describe them here.)

Experience with the Special Project framework

(Please let us know about your experience with administrative aspects like the application procedure, progress reporting etc.)

Summary of results

(This section should comprise up to 10 pages, reflecting the complexity and duration of the project, and can be replaced by a short summary plus an existing scientific report on the project.)

The following summaries highlights our use of ECMWF data during the project:

1. Black Carbon (BC) in Arctic surface and snow
2. Determination of 134Cs, 137Cs and 131I emissions using inverse modelling and an updated measurement database
3. Modelling mineral dust in the Arctic and Iceland
4. Quantifying the mass loading of particles in an ash cloud remobilized from tephra deposits on Iceland
5. Implementation, Test and Case study of a wet deposition algorithm in backward mode
6. Transport of Black Carbon (BC) in the Greenland Ice Sheet from the 2017 fires in Greenland
7. Inverse modeling of Black Carbon (BC) in high northern latitudes in 2013–2015 time period
8. Radiative forcing by mineral dust

1) Black Carbon (BC) in Arctic surface and snow

N. Evangeliou, A. Stohl

The concentrations of BC were simulated with version 10 of the LPDM FLEXPART (FLEXible PARTicle dispersion model) (Stohl et al., 2005). The model was driven with operational meteorological analyses every three hours from the European Centre for Medium-Range Weather Forecasts (ECMWF, operational fields). Computational particles released from the measurement locations were tracked back in time in FLEXPART's "retroplume" mode (Stohl et al., 2003). Simulations extended over 30 d back in time, sufficient to include most aerosol emissions arriving at the station, given a typical BC lifetime (~1 week). This enabled identifying where the measured BC came from and allowed quantification of BC source contributions. FLEXPART simulations were performed every hour during the cruise, with

particles released from small boxes covering the latitude and longitude ranges of the ship track during the hour (Fig. 1). The FLEXPART retroplumes consist of an emission sensitivity (often also called source-receptor relationship), which yields a simulated concentration in the receptor box when multiplied with gridded emissions from an inventory.

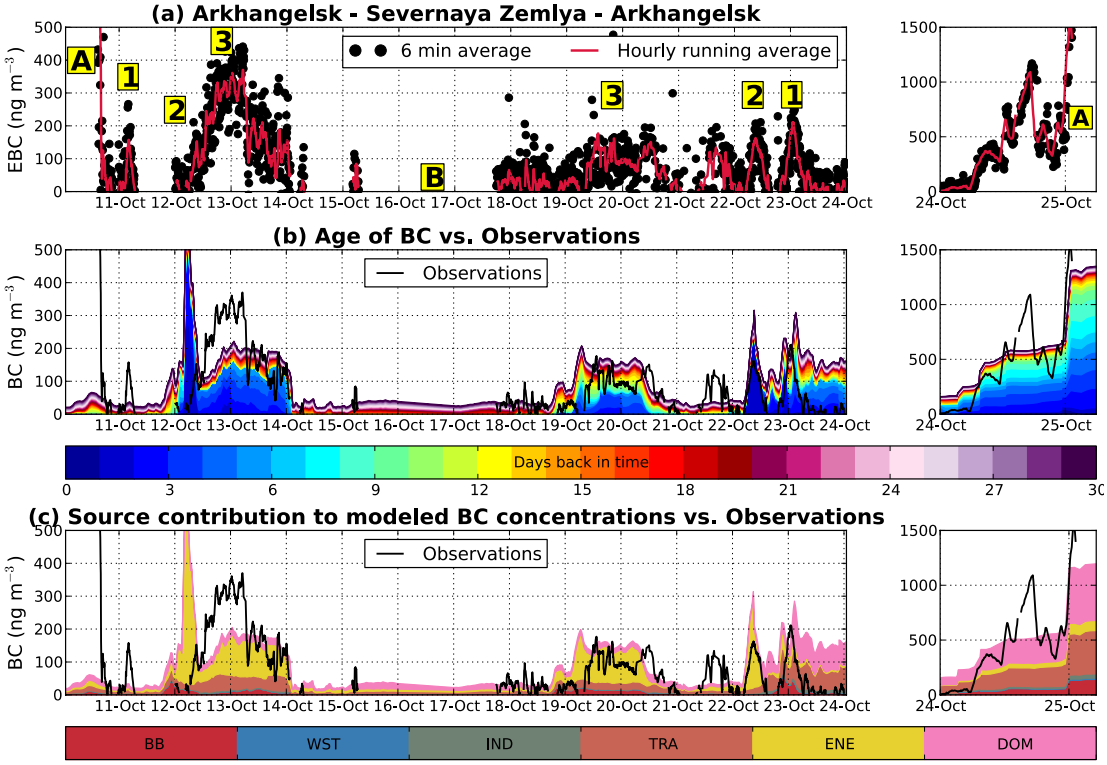

Fig. 1. (a) Time series of equivalent black carbon (EBC) during the expedition cruise. (b) Age spectra of modeled BC (colors) showing the contribution of emissions each day back in time to the surface concentration of BC. Hourly means of measured BC concentrations are shown as a black line. (c) Contribution from different emission source types to the BC surface concentrations (BB: biomass burning, WST: waste burning, IND: industrial combustion, TRA: transportation, ENE: power plants, energy conversion, and extraction, DOM: residential and commercial combustion from GFEDv3.1 and ECLIPSE inventories). More details in Popovicheva *et al.* (2017).

The simulations for the snow BC (Fig. 2) were conducted using a new feature of FLEXPART that reconstructs wet and dry deposition with backward simulations. This new feature is an extension of the aforementioned retroplume mode. To reconstruct wet deposition amounts of BC, computational particles were released at altitudes of 0 to 20 km at the locations where snow samples were taken, whereas to reconstruct dry deposition, particles were released between the surface and 30 m at these locations. All released particles together represent a unity deposition amount, which was converted immediately (i.e., upon release of a particle) to atmospheric concentrations using the deposition intensity as characterized either by dry deposition velocity or scavenging rate. The concentrations were subsequently treated as in normal retroplume backward tracking to establish emission sensitivity between the emissions and deposited amounts. The ending time of the particle release was the time at which the snow sample was collected, whereas the beginning time was set as the time when the ECMWF precipitation at the sampling site, accumulated backward in time, was equal to the water equivalent of the snow sample, up to the specified sampling depth.

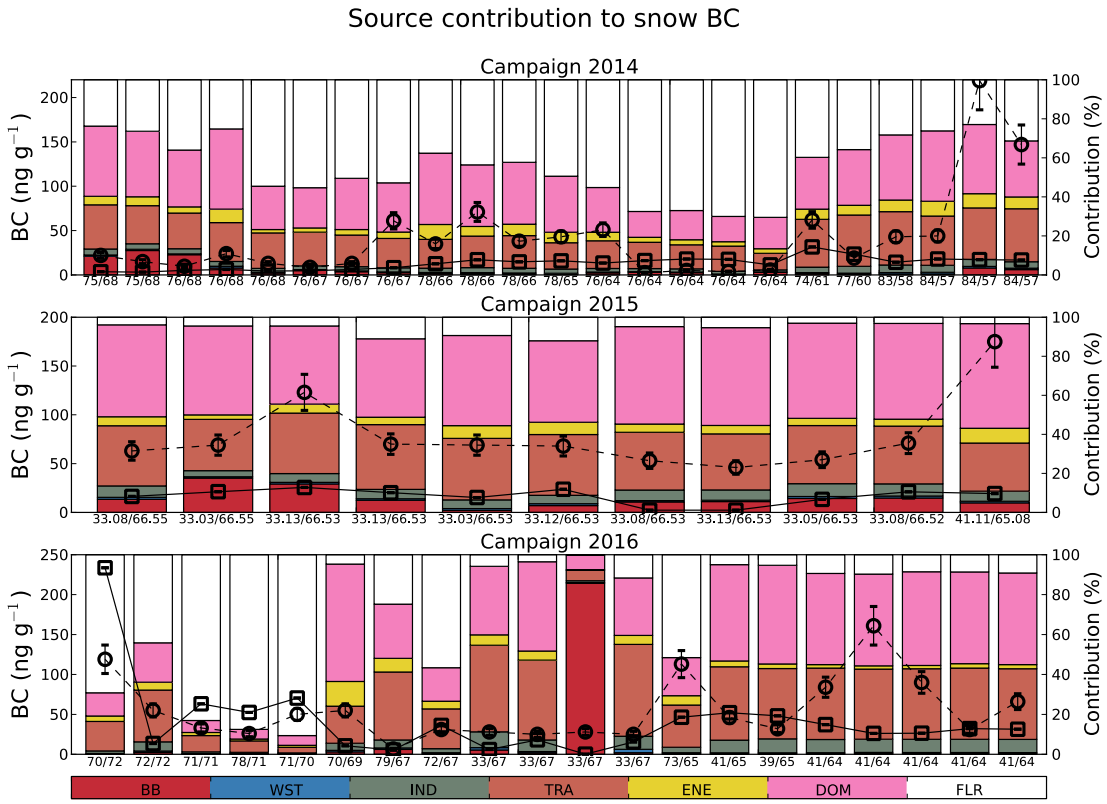

Fig. 2. Contribution from the various emission categories considered in the ECLIPSE and GFED inventories (BB: biomass burning, WST: waste burning, IND: industrial combustion, TRA: surface transportation, ENE: emissions from energy conversion, DOM: residential and commercial combustion, FLR: gas flaring) to simulated BC concentrations in snow during the 2014, 2015 and 2016 in Western Siberia and northwestern European Russia. Bars show the relative source contribution (0 –100%, right axis) and are sorted, from left to right, from the northernmost to the southernmost measurement location (coordinates are reported on the bottom as longitude/latitude). Measured EC concentrations in snow are reported with open circles, whereas modelled BC is shown with open rectangles (left axis). More details in Evangeliou *et al.* (2017).

2) Determination of ^{134}Cs, ^{137}Cs and ^{131}I emissions using inverse modelling and an updated measurement database

N. Evangeliou, T. Hamburger, A. Stohl

We have used Bayesian inversion to determine of the source term of the radionuclides ^{134}Cs, ^{137}Cs and ^{131}I released after the Chernobyl accident. The accident occurred on 26 April 1986 in the Former Soviet Union and released about 10^{19} Bq of radioactive materials that were transported as far away as the USA and Japan. Thereafter, several attempts to assess the real magnitude of the emissions were made that were based on the knowledge of the core inventory and the levels of the spent fuel. More recently, when modelling tools were further developed, inverse modelling techniques were applied to the Chernobyl case for source term quantification. However, high quality measurements, that are essential for inverse modelling, were not made available except for a few sparse activity concentration measurements far from the source and far from the main direction of the radioactive fallout. For the first time, we apply Bayesian inversion of the Chernobyl source term using not only activity concentrations, but also deposition measurements from the most recent public dataset (Evangeliou et al., 2016).

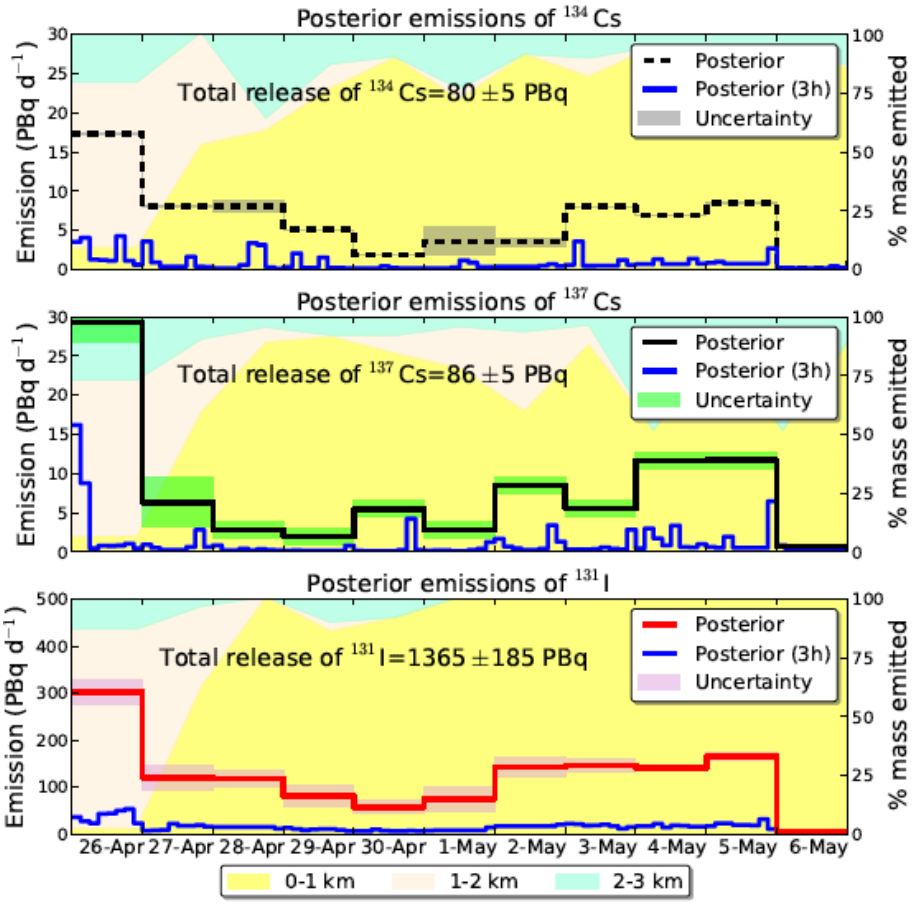

Fig. 3. Posterior emissions of ^{134}Cs, ^{137}Cs and ^{131}I against uncertainty plotted daily, as well as per time–step (3 h) from 26 April to 7 May 1986. On the right axis the vertical distribution of the emissions at altitudes 0–1 km (yellow), 1–2 km (beige) and 2–3 km (turquoise) is plotted as shaded background colours.

As regards to our inverse modelling results (Fig. 3), emissions of ^{134}Cs were estimated to be 80 PBq or 30–50 % higher than what was previously published. From the released amount of ^{134}Cs, about 70 PBq were deposited all over Europe. Similar to ^{134}Cs, emissions of 137Cs were estimated as 86 PBq, in the same order with previously reported results. Finally, ^{131}I emissions of 1365 PBq were found, which are about 10 % less than the prior total releases. The inversion pushes the injection heights of the three radionuclides to higher altitudes (up to about 3 km) than previously assumed (≈ 2.2 km) in order to better match both concentration and deposition observations over Europe. The results were of the present inversion were confirmed using an independent Eulerial model, for which deposition patterns were also improved when using the estimated posterior releases. Although the independent model tends to underestimate deposition in countries that are not in the main direction of the plume, it reproduces country levels of deposition very efficiently. The results were also tested for robustness against different set-ups of the inversion through sensitivity runs. More information can be found in Evangeliou et al. (2017a).

3) Modelling mineral dust in the Arctic and Iceland

C. Groot Zwaaftink, H. Grythe, S. Eckhardt, A. Stohl

Mobilization, atmospheric transport and deposition of mineral dust in the Arctic have been studied with FLEXPART. A module to estimate dust emission from source regions, called FLEXDUST, was developed. In this module we use meteorological fields from the European Centre for Medium-Range Weather Forecasts (ECMWF) to estimate mineral dust availability and emission. In a series of global simulations for the years 2010-2012 we analysed the seasonal variation of dust emission. Simulations showed that emission from Arctic source regions peaks in late summer/fall, likely due to limited snow cover. Atmospheric transport was calculated with FLEXPART, driven by ECMWF analysis fields. Seasonal variation of atmospheric dust load in the Arctic was strong and peak dust loads were found in spring. Dust loads were dominated by dust from remote source regions. Near the surface, however, simulations showed that local sources contribute substantially to dust concentrations and therefore dust deposition in the Arctic. Dust deposition patterns (Figure

1), reveal that transport of dust from northern high-latitude sources is limited and large fractions are deposited close to the source regions.

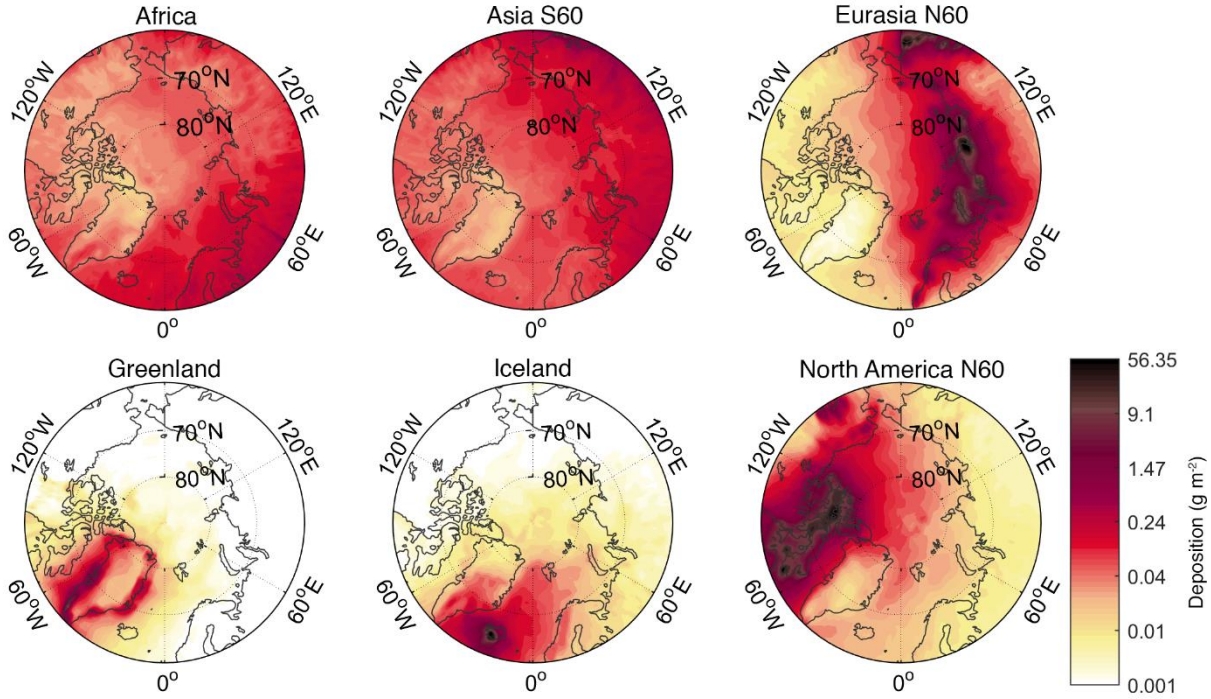

Figure 1 Simulated contribution of a selection of source regions to mean deposition of mineral dust in the Arctic in years 2010-2012 (Figure from Groot Zwaaftink et al., 2016).

Following this, we studied the high-latitude dust sources in Iceland in more detail. Here, we run FLEXDUST and FLEXPART simulations for a single year at high resolution and studied interannual variability over 27 years at a coarser resolution. For 2012, hourly ECMWF analysis data at 0.2°-resolution were used in FLEXPART simulations. The model is able to predict the timing of dust events consistent with particulate matter observations at short and long distances to the dust sources. Some inconsistencies were found for small dust sources, related to source depletion and snow cover representation. For the period 1990-2016, FLEXPART was driven with ERA Interim Reanalysis fields. These long-term simulations showed that annual dust emission from Iceland is on average about 4.3 Tg. Considering the small size of dust sources (<20.000 km^2) this is a large amount and Icelandic dust sources thus appear to be as active as parts of the Sahara. Most of the dust mobilized in Iceland is deposited in the ocean, both north-east and south of Iceland, while some dust also reaches the Greenland Ice sheet (Figure 2). Further study showed that dust deposition on glaciers in Iceland strongly affects glacier melt rates (Wittmann et al., 2017).

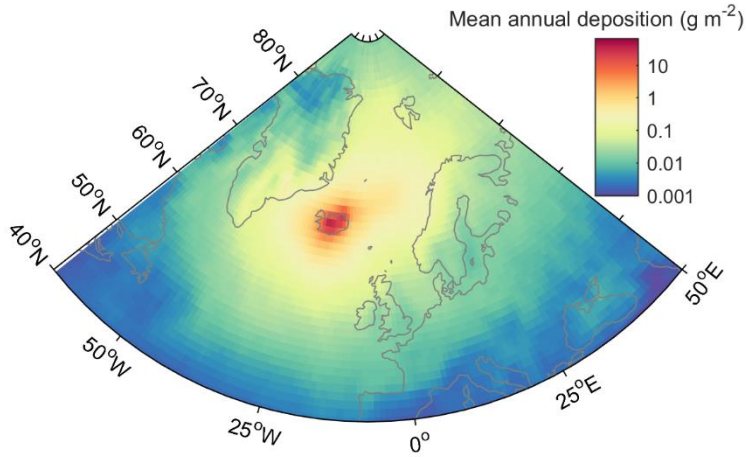

Figure 2 Simulated annual mean deposition of dust originating from Iceland in years 1990-2016 based on FLEXPART simulations (figure from Groot Zwaaftink et al., 2017).

4) Quantifying the mass loading of particles in an ash cloud remobilized from tephra deposits on Iceland

Frances Beckett , Arve Kylling , Guðmunda Sigurðardóttir, Sibylle von Löwis , and Claire Witham

On 16–17 September 2013 strong surface winds over tephra deposits in southern Iceland led to the resuspension and subsequent advection of significant quantities of volcanic ash. The resulting resuspended ash cloud was transported to the south-east over the North Atlantic Ocean and, due to clear skies at the time, was exceptionally well observed in satellite imagery. We use satellite-based measurements in combination with radiative transfer and dispersion modelling to quantify the total mass of ash resuspended during this event. Typically ash clouds from explosive eruptions are identified in satellite measurements from a negative brightness temperature difference (BTD) signal; however this technique assumes that the ash resides at high levels in the atmosphere. Due to a temperature inversion in the troposphere over southern Iceland during 16 September 2013, the resuspended ash cloud was constrained to altitudes of < 2 km a.s.l. We show that a positive BTD signal can instead be used to identify ash-containing pixels from satellite measurements. The brightness temperature (BT) varies with the amount of water vapour in the atmosphere, the atmospheric temperature profile, and the temperature of the underlying surface. For these parameters analysis data from the European Centre for Medium-Range Weather Forecasts (ECMWF) were utilized to estimate water vapour effects on the brightness temperature difference signal used to identify ash affected pixels. Examples of BTDs for the remobilization event is shown in Fig. 1. The timing and location of the ash cloud identified using this technique from measurements made by the Visible Infrared Imaging Radiometer Suite (VIIRS) on board the Suomi National Polar-orbiting Partnership (NPP) satellite agree well with model predictions using the dispersion model NAME (Numerical Atmospheric-dispersion Modelling Environment). Total column mass loadings are determined from the VIIRS data using an optimal estimation technique which accounts for the low altitude of the resuspended ash cloud and are used to calibrate the emission rate in the resuspended ash scheme in NAME. The column mass loading retrieval used look-up-tables calculated using area-averaged ECMWF water vapour, pressure and temperature profiles . Considering the tephra deposits from the recent eruptions of Eyjafjallajökull and Grímsvötn as the potential source area for resuspension for this event, we estimate that ~ 0.2 Tg of ash was remobilized during 16–17 September 2013.

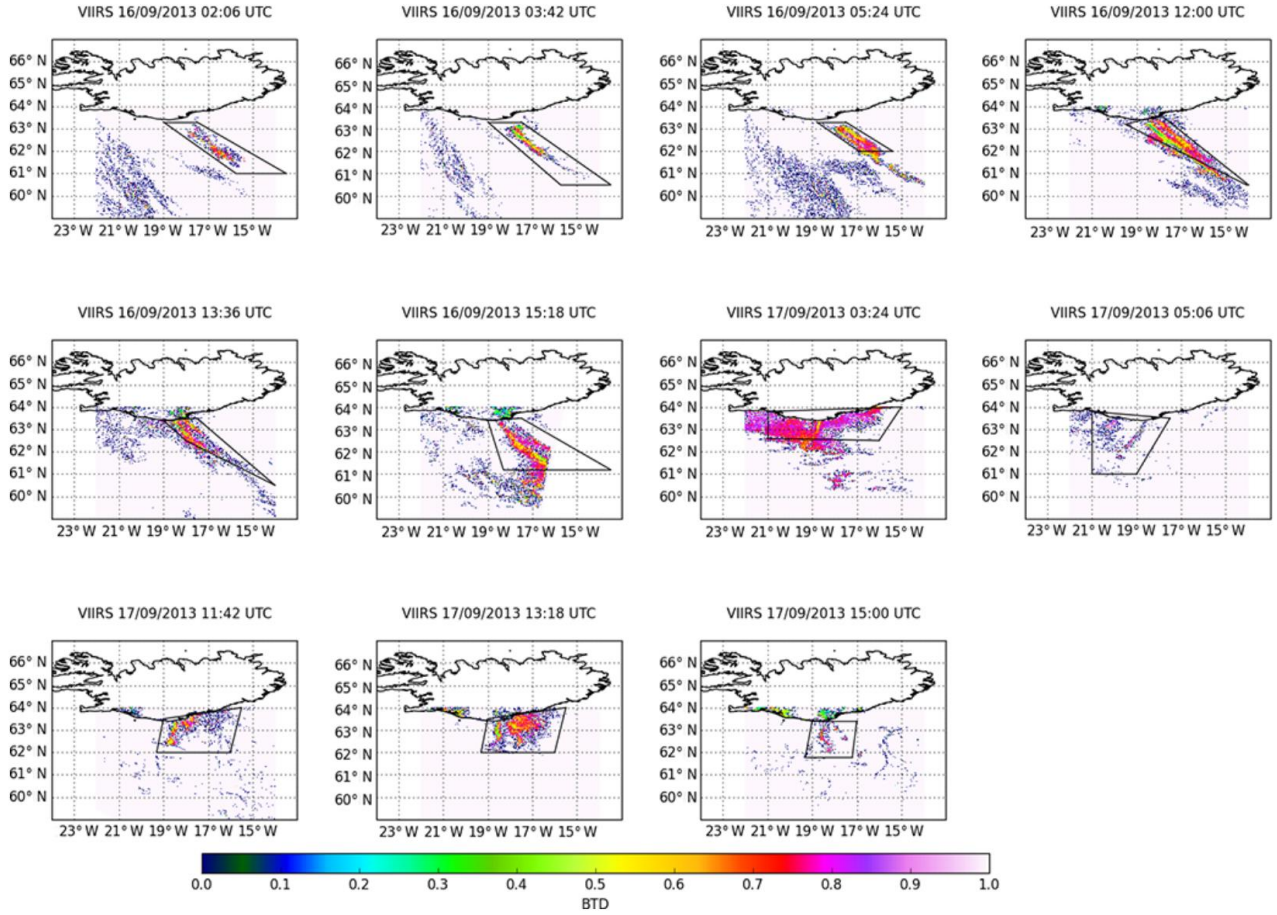

Figure 1. VIIRS BTDs for pixels identified as resuspended ash, 16–17 September 2013.

5) Implementation, Test and Case study of a wet deposition algorithm in backward mode.

Existing Lagrangian particle dispersion models are capable of establishing source-receptor relationships by running either forward or backward in time. For receptor-oriented studies such as interpretation of "point" measurement data, backward simulations can be computationally more efficient by several orders of magnitude. However, to date, the backward modelling capabilities have been limited to atmospheric concentrations or mixing ratios. We extend the backward modelling technique to substances deposited at the Earth's surface by wet scavenging and dry deposition. This facilitates efficient calculation of emission sensitivities for deposition quantities at individual sites, which opens new application fields such as the comprehensive analysis of measured deposition quantities, or of deposition recorded in snow samples or ice cores. This could also include inverse modelling of emission sources based on such measurements. We have tested the new scheme as implemented in the Lagrangian particle dispersion model FLEXPART v10.2 by comparing results from forward and backward calculations.

For this study, we used three-hourly ERA-Interim re-analysis data from ECMWF with a resolution of 1˚ latitude x 1˚ longitude and 61 vertical levels. Figure 1 shows the emission flux of the inventory used (Fig. 1a), the average concentration in the lowest model layer (0-100 m above ground level) (Fig. 1b), and the accumulated wet (Fig. 4c) and dry deposition (Fig. 1d) for March 2012. Based on these results, we selected two locations where we compare the results for forward and backward simulations. The two points represent very different concentration and deposition levels, due to their different distances from strong BC source regions. While point A is located relatively close to strong emission sources (average concentration of 270 ng m-3), point B on Spitsbergen in the Arctic is far away from sources (average concentration of 7 ng m-3) .

In general, the forward and backward simulations show very good agreement for both receptor points. For example, the distinct daily cycles in concentration and dry deposition at point A are simulated similarly, and the mean concentration and deposition values are almost identical in the forward and backward simulations at both points. However, during some episodes there can be notable differences, for example at the end of the simulation period at point A.

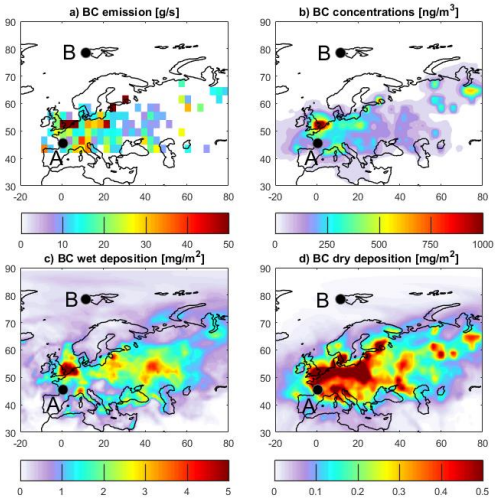

Figure 1: Average BC emission fluxes (a), average BC concentrations in the lowest model layer (0-100 m) (b), accumulated BC wet deposition (c) and accumulated BC dry deposition (d) for the period of 1 March to 1 April 2012. The black dots show the locations A and B for which a detailed comparison of forward and backward calculations is performed.

6) Transport of Black Carbon (BC) in the Greenland Ice Sheet from the 2017 fires in Greenland

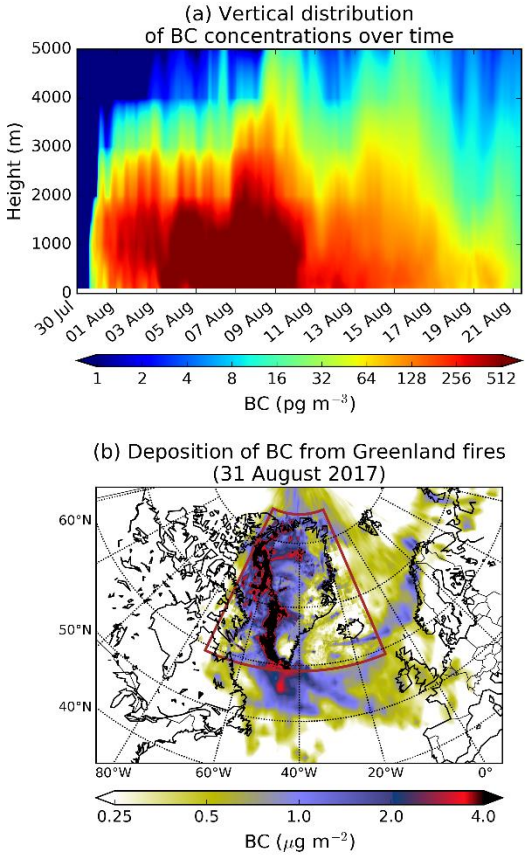

Figure 2. (a) Time-series of vertical distribution of BC concentrations averaged over the area of Greenland in summer 2017 as a function of time. (b) Total (wet and dry) deposition of BC (in µg m-2) from Greenland fires until 31 August 2017. The colored rectangle depicts the nested high-resolution domain.

We simulated highly-unusual open fires that burned in Western Greenland between 31 July and 21 August 2017, after a period of warm, dry and sunny weather. The fires burned on peat lands that became vulnerable to fires by permafrost thawing. We used several satellite data sets to estimate that the total area burned was about 2345 hectares. Based on assumptions of typical burn depths and BC emission factors for peat fires, we estimate that the fires consumed a fuel amount of about 117 kt C and produced BC emissions of about 23.5 t. We used the Lagrangian particle dispersion model FLEXPART to simulate the atmospheric BC transport and deposition (Figure 2) driven by hourly 0.5°×0.5° operational analyses from the European Centre for Medium-Range Weather Forecasts (ECMWF). Concentration and deposition fields were recorded in a global domain of 1°×1° spatial resolution with three hourly outputs. To capture the spatiotemporal variability of BC over the Greenland Ice Sheet, a nested domain with 0.05°×0.05° resolution was used. We find that the smoke plumes were often pushed towards the Greenland Ice Sheet by westerly winds and thus a large fraction of the BC emissions (7 t or 30%) was deposited on snow or ice covered surfaces. The calculated BC deposition was small compared to BC deposition from global sources, but not entirely negligible.

7) Inverse modeling of Black Carbon (BC) in high northern latitudes in 2013–2015 time period

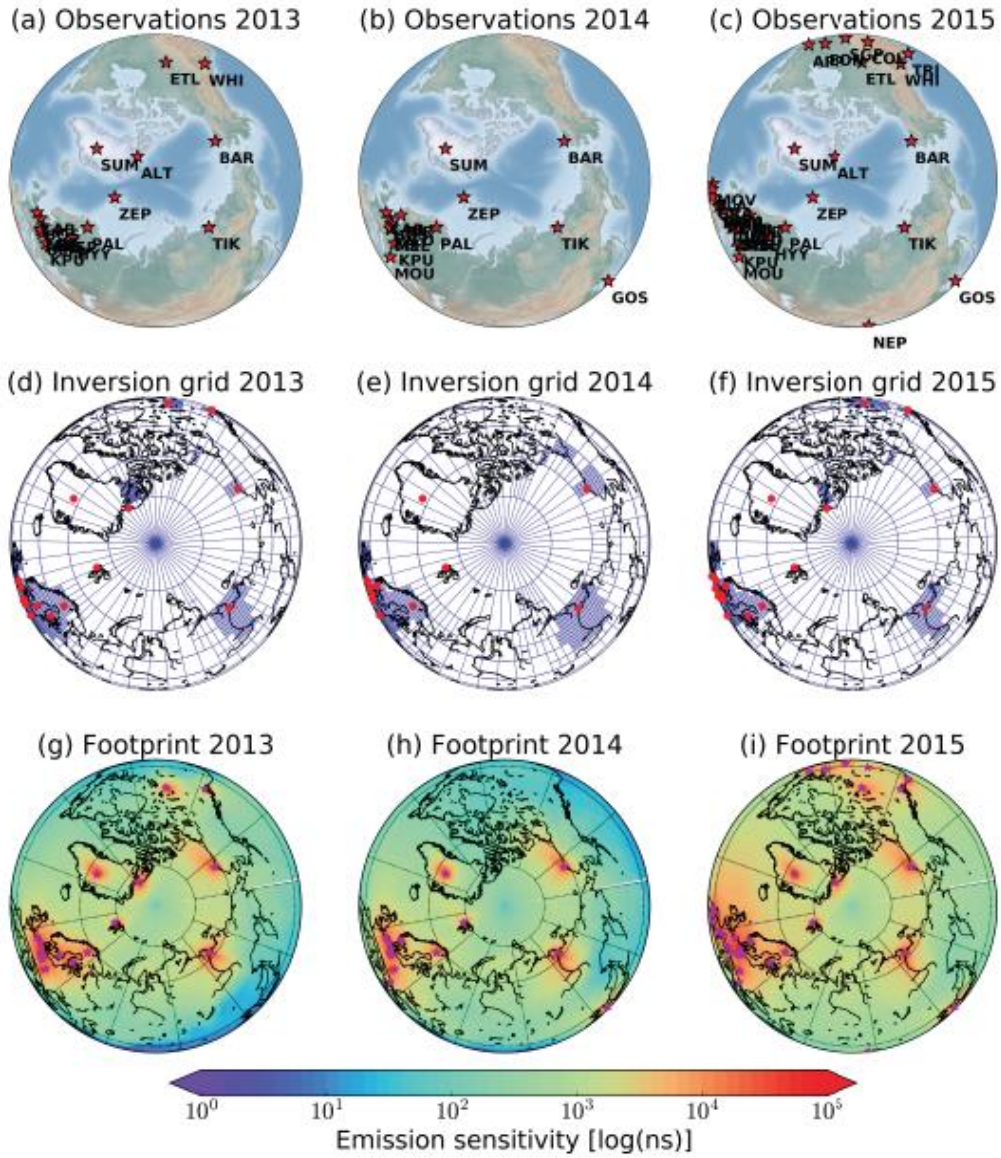

Figure 3. Observation network used for the present inversion (a, b and c), and variable-resolution grid used for the inversion (d, e, and f) also showing the location of the observation sites (red stars) for 2013–2015 period. Sensitivity to the surface emissions (i.e., the footprint emission sensitivity or equivalently source-receptor relationship) integrated over all observation sites and all time steps (g, h and i) for the years 2013, 2014 and 2015 (units of log(ns)).

We conducted BC inversions at high northern latitudes (>50°N) for the 2013–2015 period. A sensitivity analysis was performed to select the best representative species for BC and the best prior emission dataset. The same model ensemble was used to assess the uncertainty of the posterior emissions of BC due to scavenging and removal and due to the use of different prior emission inventory. The source-receptor relationships for the Bayesian inversion were calculated using the Lagrangian particle dispersion model FLEXPART driven with European Centre for Medium-Range Weather Forecasts operational meteorological analyses from the Integrated Forecast System (IFS) with 137 model levels and a horizontal resolution of 0.5°×0.5°. The optimised emissions of BC were high close to the gas flaring regions in Russia and in Western Canada (Alberta), where numerous power and oil/gas production industries operate. The annual posterior emissions of BC at latitudes above 50°N were estimated as 560±171 kt yr-1, significantly smaller than in ECLIPSEv5 (745 kt yr-1), which was used and the prior information in the inversions of BC. The average relative uncertainty of the inversions was estimated to be 30%.

Posterior concentrations of BC simulated over Arctic regions were compared with independent observations from flight and ship campaigns showing, in all cases, smaller bias, which in turn witnesses the success of the inversion. Posterior emissions of BC in North America are driven by anthropogenic sources, while biomass burning appeared to be less significant as it is also confirmed by satellite products. In North Europe, posterior emissions were estimated to be half compared to the prior ones, with the highest releases to be in megacities and due to biomass burning in Eastern Europe. The largest emissions of BC in Siberia were calculated along the transect between Yekaterinsburg and Chelyabinsk. Flaring emissions in Nenets-Komi oblast (Russia) were estimated to be much lower than in the prior emissions, while in

Khanty-Mansiysk (Russia) they remained the same after the inversions of BC. Increased emissions in the borders between Russia and Mongolia are probably due to biomass burning in villages along the Trans-Siberian Railway.

8) Radiative forcing by mineral dust

Mineral dust sources at high and low latitudes contribute to atmospheric dust loads and dust deposition in the Arctic. With dust load estimates from Groot Zwaaftink et al. (2016), we quantify the mineral dust instantaneous radiative forcing (IRF) in the Arctic for the year 2012. The full study was presented by Kylling et al. (2018). Meteorological input data for simulations with the dust emission model FLEXDUST, the atmospheric transport model FLEXPART and the radiative transfer model libRadtran were ECMWF operational analysis fields at 1 degree resolution. Results show that the annual-mean top of the atmosphere IRF is 0.225 W m-2, with the largest contributions from dust transported from Asia south of 60°N and Africa (see Fig. 4). High-latitude (>60°N) dust sources contribute about 39% to top of the atmosphere IRF and have a larger impact (1 to 2 orders of magnitude) on IRF per emitted kilogram of dust than low-latitude sources. Mineral dust deposited on snow accounts for nearly all of the bottom of the atmosphere IRF of 0.135 W m-2. More than half of the bottom of the atmosphere IRF is caused by dust from high-latitude sources, indicating substantial regional climate impacts rarely accounted for in current climate models.

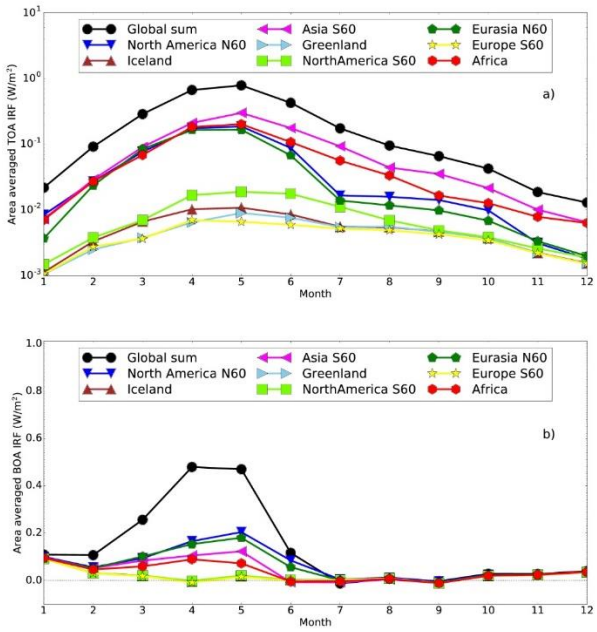

Figure 4: Individual contributions from various regions to the top of the atmosphere (TOA) (a) and bottom of the atmosphere (BOA) (b) dust instantaneous radiative forcing (IRF) for the year 2012. Note the logarithmic scale on y axis in panel (a). The black dotted line in panel (b) indicates the zero line. Figure 3 from Kylling et al. (2018).

List of publications/reports from the project with complete references

Popovitseva, O. B., Evangeliou, N., Eleftheriadis, K., Kalogridis, A. C., Sitnikov, N., Eckhardt, S., and Stohl A.: Black Carbon Sources Constrained by Observations in the Russian High Arctic, Environ. Sci.Technol., 51 (7), 3871–3879, doi:10.1021/acs.est.6b05832, 2017.

Xu, J., Martin, R. V., Morrow, A., Sharma, S., Huang, L., Leaitch, W. R., Burkart, J., Schulz, H., Zanatta, M., Willis, M. D., Henze, D. K., Lee, C. J., Herber, A. B., and Abbatt, J. P. D.: Source attribution of Arctic black carbon constrained by aircraft and surface measurements, Atmos. Chem. Phys. Discuss., https://doi.org/10.5194/acp-2017-236, 2017.

Evangeliou, N., Hamburger, T., Cozic, A., Balkanski, Y., and Stohl, A.: Inverse modelling of the Chernobyl source term using atmospheric concentration and deposition measurements, Atmos. Chem. Phys. Discuss., https://doi.org/10.5194/acp-2017-330, 2017.

Evangeliou, N., Shevchenko, V. P., Yttri, K. E., Eckhardt, S., Sollum, E., Pokrovsky, O. S., Kobelev, V. O., Korobov, V. B., Lobanov, A. A., Starodymova, D. P., Vorobiev, S. N.,

Thompson, R. L., and Stohl, A.: Origin of elemental carbon in snow from Western Siberia and northwestern European Russia during winter–spring 2014, 2015 and 2016, Atmos. Chem. Phys. Discuss., https://doi.org/10.5194/acp-2017-542, 2017.

Thompson, R. L., Sasakawa, M., Machida, T., Aalto, T., Worthy, D., Lavric, J. V., Lund Myhre, C. and Stohl, A.: Methane fluxes in the high northern latitudes for 2005-2013 estimated using a Bayesian atmospheric inversion, Atmospheric Chemistry and Physics, 17(5), 3553-3572, doi:10.5194/acp-17-3553-2017, 2017

Groot Zwaaftink, C.D. Ó. Arnalds, P. Dagsson-Waldhauserova, S. Eckhardt, J. M. Prospero, A. Stohl (2017), Temporal and spatial variability of Icelandic dust emission and atmospheric transport, under review for Atmospheric Chemistry and Physics. DOI:10.5194/acp-2017-290

Wittmann, M., C. D. Groot Zwaaftink, L. Steffensen Schmidt, S. Guðmundsson, F. Pálsson, O. Arnalds, H. Björnsson, T. Thorsteinsson, and A. Stohl (2017), Impact of dust deposition on the albedo of Vatnajökull ice cap, Iceland, The Cryosphere, 11(2), 741-754. DOI:10.5194/tc-11-741-2017

Groot Zwaaftink, C. D., H. Grythe, H. Skov and A. Stohl (2016), Substantial contribution of northern high-latitude sources to mineral dust in the Arctic, Journal of Geophysical Research, 121, DOI: 10.1002/2016JD025482

Beckett, F., Kylling, A., Sigurðardóttir, G., von Löwis, S. and Witham, C., 'Quantifying the mass loading of particles in an ash cloud remobilized from tephra deposits on Iceland', Atmospheric Chemistry and Physics, 7, 17, 4401-4418, http://www.atmos-chem-phys.net/17/4401/2017/, doi:10.5194/acp-17-4401-2017, 2017.

Eckhardt, S., M. Cassiani, N. Evangeliou, E. Sollum, I. Pisso, and A. Stohl (2017): Source-receptor matrix calculation for deposited mass with the Lagrangian particle dispersion model FLEXPART v10.2 in backward mode. Geophys. Mod. Dev. 10, 4605-4618, doi:10.5194/gmd-10-4605-2017

Evangeliou, N., Kylling, A., Eckhardt, S., Myroniuk, V., Stebel, K., Paugam, R., Zibtsev, S., and Stohl, A.: Open fires in Greenland: an unusual event and its impact on the albedo of the Greenland Ice Sheet, Atmos. Chem. Phys. Discuss., https://doi.org/10.5194/acp-2018-94, in review, 2018.

Evangeliou, N., Thompson, R. L., Eckhardt, S., and Stohl, A.: Top–down estimates of black carbon emissions at high latitudes using an atmospheric transport model and a Bayesian inversion framework, Atmos. Chem. Phys. Discuss. submitted, 2018.

Groot Zwaaftink, C. D., H. Grythe, H. Skov, A. Stohl, (2016) Substantial contribution of northern high-latitude sources to mineral dust in the Arctic, Journal of Geophysical Research, 121, 13,678–13,697, DOI: 10.1002/2016JD025482

Kylling A., C.D. GrootZwaaftink, and A. Stohl (2018), 'Mineral dust instantaneous radiative forcing in the Arctic', Geophys. Res. Lett., 45, doi:10.1029/2018GL077346.

Evangeliou, N., Kylling, A., Eckhardt, S., Myroniuk, V., Stebel, K., Paugam, R., Zibtsev, S., and Stohl, A. (2019): Open fires in Greenland in summer 2017: transport, deposition and radiative effects of BC, OC and BrC emissions, Atmos. Chem. Phys., 19, 1393-1411, https://doi.org/10.5194/acp-19-1393-2019,

Mühle, J., Trudinger, C. M., Western, L. M., Rigby, M., Vollmer, M. K., Park, S., Manning, A. J., Say, D., Ganesan, A., Steele, L. P., Ivy, D. J., Arnold, T., Li, S., Stohl, A., Harth, C. M., Salameh, P. K., McCulloch, A., O'Doherty, S., Park, M.-K., Jo, C. O., Young, D., Stanley, K. M., Krummel, P. B., Mitrevski, B., Hermansen, O., Lunder, C., Evangeliou, N., Yao, B., Kim, J., Hmiel, B., Buizert, C., Petrenko, V. V., Arduini, J., Maione, M., Etheridge, D. M., Michalopoulou, E., Czerniak, M., Severinghaus, J. P., Reimann, S., Simmonds, P. G., Fraser, P. J., Prinn, R. G., and Weiss, R. F. (2019), "Perfluorocyclobutane (PFC-318, c-C4F8) in the global atmosphere", Atmospheric Chemistry & Physics, 19, 10335–10359, https://doi.org/10.5194/acp-19-10335-2019.

Vargas, A., Arnold, D., Duch, M.-A., Evangeliou, N., Sievers, K., and Maurer, C. (2019), "Dose calculations in aircrafts after Fukushima nuclear power plant accident–Preliminary study for aviation operations", Journal of Environmental Radioactivity, 205-206, 24-33, https://doi.org/10.1016/j.jenvrad.2019.04.013.

Winiger, P., Barrett, T. E., Sheesley, R. J., Huang, L., Sharma, S., Barrie, L. A., Yttri, K. E., Evangeliou, N., Eckhardt, S., Stohl, A., Klimont, Z., Heyes, C., Semiletov, I. P., Dudarev, O. V., Charkin, A., Shakhova, N., Holmstrand, H., Andersson, A., and Gustafsson, Ö. (2019), "Source apportionment of circum-Arctic atmospheric black carbon from isotopes and modeling", Science Advances, 5 (2), eaau8052, https://doi.org/10.1126/sciadv.aau8052

Future plans

(Please let us know of any imminent plans regarding a continuation of this research activity, in particular if they are linked to another/new Special Project.)